

# AIRBORNE INFRARED-HYPERSPECTRAL MAPPING FOR DETECTION OF GASEOUS AND SOLID TARGETS

**Eldon Puckrin, Caroline-Stéphanie Turcotte, Pierre Lahaie and Denis Dubé**

Defence R&D Canada – Valcartier  
2459 Pie-XI Blvd N., Québec, QC, Canada G3J 1X5  
[eldon.puckrin@drdc-rddc.gc.ca](mailto:eldon.puckrin@drdc-rddc.gc.ca)

**Vincent Farley, Philippe Lagueux, Frédérick Marcotte and Martin Chamberland**

Telops Inc.  
100-2600 St-Jean-Baptiste, Québec, QC, Canada G2E 6J5  
[vincent.farley@telops.com](mailto:vincent.farley@telops.com)

## ABSTRACT

Airborne hyperspectral ground mapping is being used in an ever-increasing extent for numerous applications in the military, geology and environmental fields. The different regions of the electromagnetic spectrum help produce information of differing nature. The visible, near-infrared and short-wave infrared radiation (400 nm to 2.5  $\mu\text{m}$ ) has been mostly used to analyze reflected solar light, while the mid-wave (3 to 5  $\mu\text{m}$ ) and long-wave (8 to 12  $\mu\text{m}$  or thermal) infrared senses the self-emission of molecules directly, enabling the acquisition of data during night time.

The Telops Hyper-Cam is a rugged and compact infrared hyperspectral imager based on the Fourier-transform technology. It has been used on the ground in several field campaigns, including the demonstration of standoff chemical agent detection. More recently, the Hyper-Cam has been integrated into an airplane to provide airborne measurement capabilities. The technology offers fine spectral resolution (up to 0.25  $\text{cm}^{-1}$ ) and high accuracy radiometric calibration (better than 1 degree Celsius). Furthermore, the spectral resolution, spatial resolution, swath width, integration time and sensitivity are all flexible parameters that can be selected and optimized to best address the specific objectives of each mission.

The system performance and a few measurements have been presented in previous publications. This paper focuses on analyzing additional measurements in which detection of fertilizer and Freon gas has been demonstrated.

## INTRODUCTION

Emerging applications in Defense and Security require sensors with state-of-the-art sensitivity and capabilities. Among these sensors, the imaging spectrometer is an instrument yielding a large amount of rich information about the measured scene. This powerful spectrometric tool is becoming more common in civil applications such as search and rescue, geological surveys, pollution monitoring, forest fire detection and monitoring and combustion studies. These sensors are now also emerging as indispensable assets for defence operations through the role they can play for troop protection against chemical attacks, detection of mines and unexploded ordnance (UXO) and for the detection of camouflaged targets. Imaging spectrometers have unmatched capabilities to meet the requirements of these applications.

Telops has developed the Hyper-Cam-LW and Hyper-Cam-MW hyperspectral imagers. The former operates in the 8-12  $\mu\text{m}$  longwave infrared (LWIR) spectral range and the latter in the 3-5  $\mu\text{m}$  midwave infrared (MWIR) spectral range, with an extendable option to shorter wavelength. The Hyper-Cam is based on the Fourier-transform technology yielding high spectral resolution and enabling high-accuracy radiometric calibration. The Hyper-Cam, a portable sensor, provides datacubes of up to 320x256 pixels at 0.35 mrad spatial resolution and at spectral resolutions of up to 0.25 $\text{cm}^{-1}$ . The Hyper-Cam-LW has been used in several ground-based field campaigns, including the demonstration of standoff chemical agent detection (Farley, 2007).

The Hyper-Cam-LW was first flown in its airborne configuration during the winter of 2008 (Puckrin, 2009). Under very difficult winter conditions with low thermal contrast, the Hyper-Cam-LW was able to detect gas plumes of SF<sub>6</sub>. In addition, the airborne Hyper-Cam-LW was used to map a Canadian industrial site where plumes of SO<sub>2</sub> were readily detected and identified. The current paper focuses on results from a recent springtime trial held at Defence R&D Canada – Valcartier under more hospitable environmental conditions. Experiments involving chemical gas releases, fertilizer targets and disturbed earth were set up, and a number of overpasses were performed with the airborne Hyper-Cam.

## HYPER-CAM SENSOR DESCRIPTION

The Hyper-Cam is a lightweight and compact imaging radiometric spectrometer. The spectral measurements are performed using a Fourier-transform spectrometer (FTS), which incorporates a 320x256 focal plane array detector that can be windowed and formatted to fit the desired image size and to decrease the acquisition time. Both, MCT and InSb focal plane arrays are used to cover the LWIR and the MWIR bands, respectively. Spectral resolution is user selectable and ranges from 0.25 to 150  $\text{cm}^{-1}$ . This instrument generates a complete spectrum of each pixel in the image, with each pixel having an instantaneous field-of-view of 0.35 mrad. This field-portable sensor is shown in Figure 1.

The instrument has two internal calibration blackbodies used to perform an end-to-end radiometric calibration of the infrared measurements. The sensor also has advanced acquisition and processing electronics, offering the capability to convert the raw interferograms into spectra using a real-time discrete-Fourier transform (DFT), and also offering the capability to apply the radiometric calibration, generating for output real-time calibrated spectra in radiance units.



**Figure 1.** Hyper-Cam hyperspectral camera.

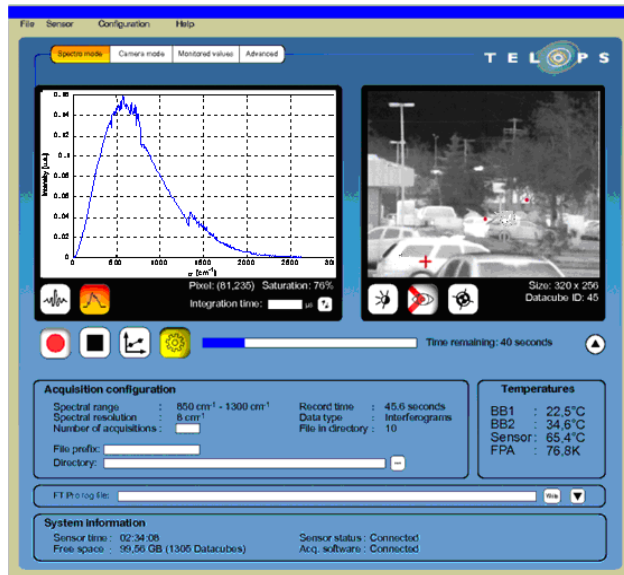


**Figure 2.** FTPro gives the operator real-time feedback: the IR image and the spectrum of a selected pixel.

The control software has a user-friendly interface and provides real-time feedback to the operator. A screenshot of the control software (named FTPro) is presented in Figure 2. On the right, the non-uniformity corrected broadband IR image is displayed with a greyscale code where black means low radiance level and white high radiance level. The uncalibrated raw spectrum (or the interferogram as selected by the operator) of a selected pixel in the image is displayed in real time on the left of the screen.

The sensor has the capability to change the focus of the IR image to produce a clear image from 3 meters up to infinity.

The Hyper-Cam was presented in detail in previous papers (Farley, 2007 & Vallieres, 2005). It has been successfully used during several field trials.

## AIRBORNE CONFIGURATION

### Design Considerations

Before it is transformed into a spectrum, the data acquired by a FTS is initially an interferogram. It is required that all the samples in the interferogram be acquired from a stationary scene; otherwise the Fourier transform of the interferogram generates errors in the spectrum. In an airborne configuration, staring at a fixed scene can become a challenge, especially for high resolution spectra, that require long interferograms. The difficulty is primarily caused by the aircraft displacement, but it also originates from the plane variations in the yaw, pitch and roll orientations, as defined in Figure 3.

From this point, one can consider two options to address the stationary scene requirement:

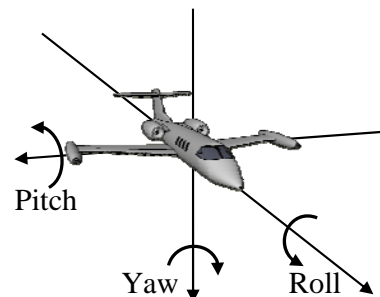


**Figure 3.** Airplane angular orientations.

1. Reduce acquisition parameters, such as the image size and the spectral resolution, in order to minimize the interferogram acquisition period and thus become less sensitive to aircraft displacement and angular movement.
2. Stare at the same ground area by using an image motion compensation (IMC) mirror that compensates the aircraft displacement and its angular movement.

The second method is preferred, as it enables better spectral resolution. Figure 4 depicts the acquisition routine of a configuration where the instrument viewing angle compensates for the aircraft displacement. By using the IMC mirror, one can acquire large 2-D images that cover several pixel lines. Also, in order to facilitate the eventual mosaicking of the different ground sections, one can adjust its scanning parameters in order to allow consecutive images to overlap.

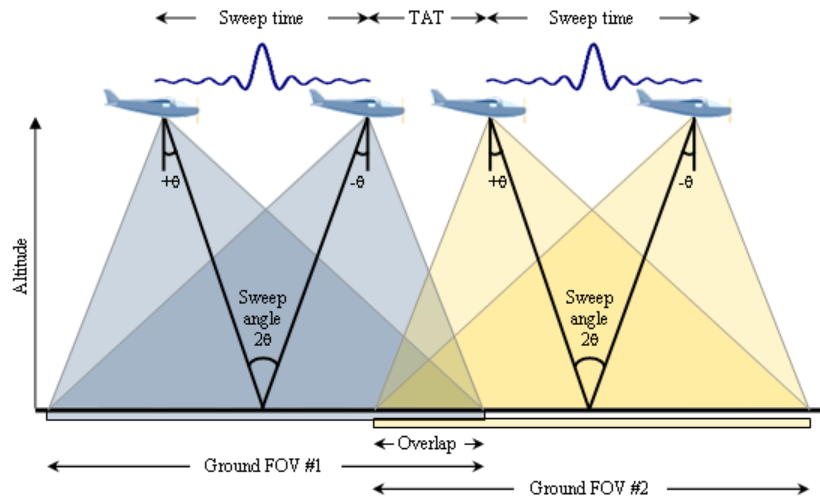


**Figure 4.** Interferogram acquisition in airborne configuration.

### System Configuration

The Hyper-Cam airborne system comprises the Hyper-Cam instrument along with several modules. The primary function of the assembly is to compensate for the aircraft displacement and its angular pitch, roll and yaw. It also adds accurate aircraft position and attitude data to the acquisition file metadata in order to later geo-reference the acquired data. The following section describes the role of each subsystem to fulfill the flight requirements.

In order to acquire the most useful infrared spectral ranges, the Telops airborne system allows mounting two different Hyper-Cam instruments. The Hyper-Cam-MW measures from 3 to 5.5  $\mu\text{m}$  whereas the Hyper-Cam-LW measures the 8 to 11.5  $\mu\text{m}$  wavelength range. The optical bench includes a stabilization platform, the two Hyper-Cam instruments, two IMC mirrors, a GPS/INS unit and two visible boresight cameras. All these modules are rigidly mounted on a high-stiffness base plate. This base plate is mounted on the stabilization platform. Figure 5 illustrate the Hyper-Cam airborne configuration.



**Figure 5.** Illustration of the airborne configuration with two Hyper-Cams.

The IMC mirrors are used to compensate the airplane pitch, roll and forward motion (independently for each Hyper-Cam sensor), while the stabilization platform is used to dampen the airplane vibrations and to compensate the airplane yaw. The IMC mirrors are controlled by the navigation module which receives and uses the information from two video trackers (one from each Hyper-Cam) and a GPS/INS unit. The GPS/INS also enables ortho-rectification and geo-referencing of the collected data.

The Hyper-Cam instruments offer uncommon flexibility in adjusting their spatial, spectral and temporal parameters. This flexibility proves to be invaluable for airborne applications where the flight parameters impose severe restrictions on spectrometer operation. Additional details on the Hyper-Cam airborne system design are provided in (Allard, 2008).

## AIRBORNE DETECTION AND IDENTIFICATION OF PLUMES AND SOLIDS

An experiment was set up at DRDC Valcartier to primarily test the capability of the airborne Hyper-Cam-LW sensor for detecting gas plumes and chemical powders under springtime clear sky conditions. The DRDC experiment was carried out on April 30, 2009. The experiments and their results are summarized in the next sub-sections.

A schematic diagram of the experimental setup used at DRDC Valcartier to perform tests on the airborne Hyper-Cam is shown in Figure 4. The ground targets consisted of a 2m × 2m wooden tray of ammonium sulphate fertilizer, a portable plume generator capable of emitting F134a gas at a maximum rate of 150 L/min, and a patch of disturbed soil (shown in Figs. 5 A,B,C), which were all installed on a gravel roadway. An ensemble of hot plates were also set up and operated at a temperature of about 150 oC, as shown in Fig. 6. In addition, targets consisting of 2m × 2m black, white and reflective panels, as shown in Fig. 7, were installed to derive the required radiative parameters for use in atmospheric compensation techniques. The sky conditions varied from mostly clear to a mix of sun and cloud. Four passes of the airborne Hyper-Cam-LW were made over the DRDC experiment, as shown in Table 1, which also summarizes the gas release plan. The LWIR signatures of the F134a gas and fertilizer are shown in Figure 8. The meteorological conditions were measured with a weather station (MWS 9-5, Reinhardt GmbH), as shown in Fig. 9, and the measured parameters are summarized in Table 2.

**Table 1.** Release rates of F134a during the aircraft overpasses.

Pass	F134a release rate (L/min)	Time (local)	Comments
1	blank	16:07	Background only
2	100	16:17	Mixed sky
3	150	16:47	30 °C background temperature
4	150	17:00	

**Target Layouts: 30 April 2009**

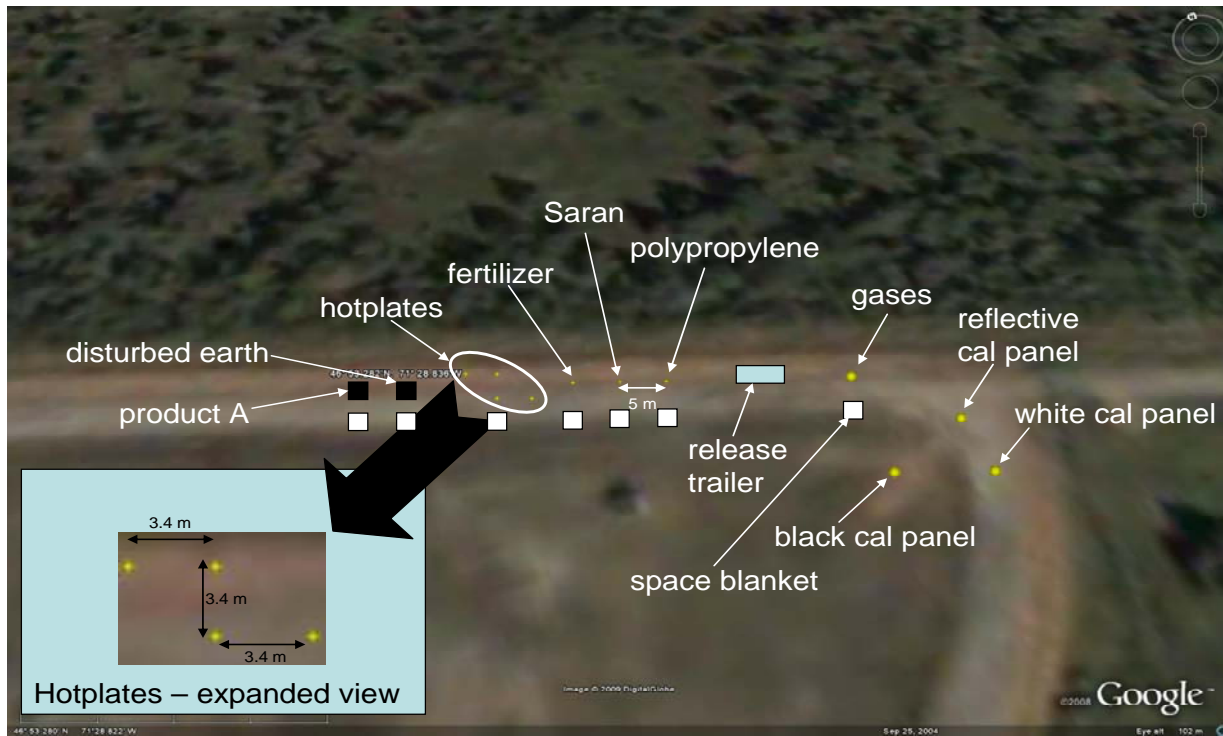


**Figure 4.** Experimental setup used on April 30 to test the Hyper-Cam-LW sensor’s airborne capability for detecting gaseous and solid chemical targets. The white squares represent 1m × 1m reflective targets used to help identify the features in the airborne imagery.

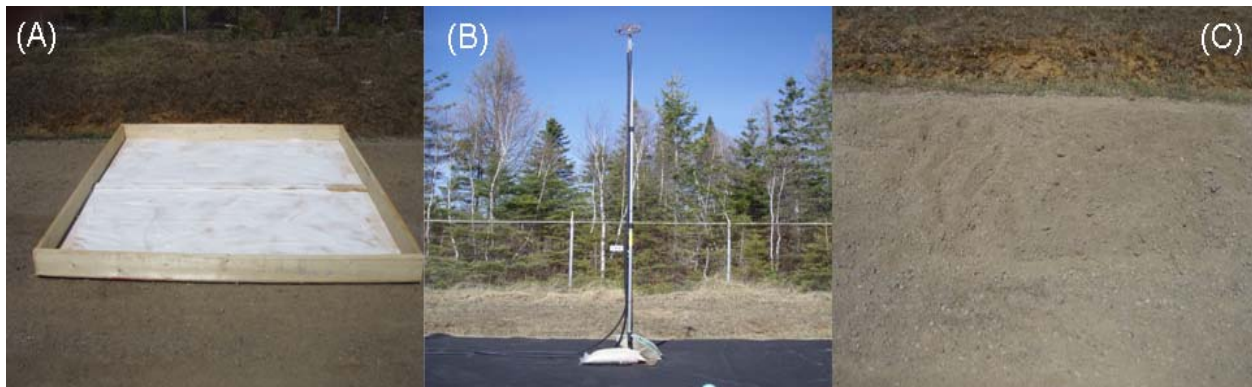


**Figure 5.** Photographs of the ground targets used in the experiment : (1) ammonium sulphate fertilizer, (2) vent used to release F134a with a black background, (3) a 1m × 1m patch of disturbed soil.





**Figure 6.** Ensemble of 4 hotplates used to test pixel size definition.

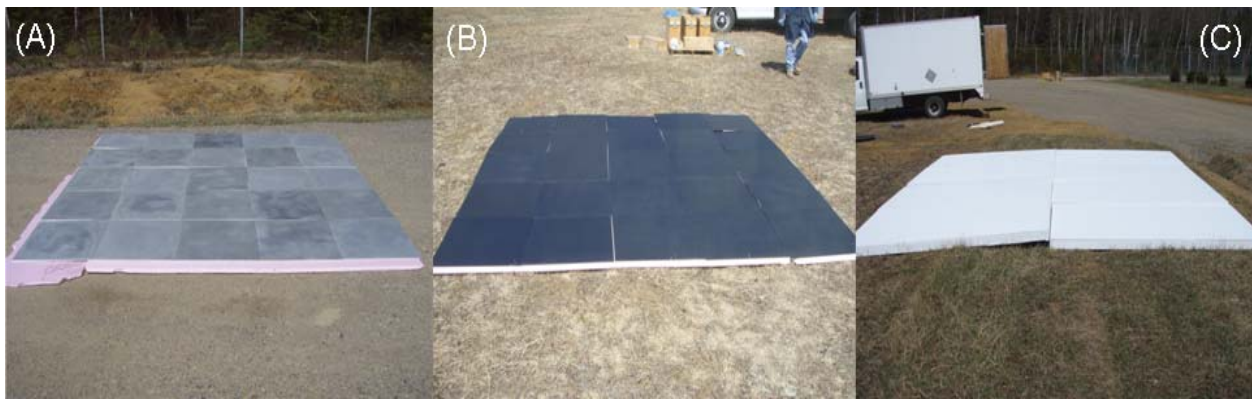


**Figure 7.** Photographs of (A) reflective, (B) black painted and (C) white painted calibration targets

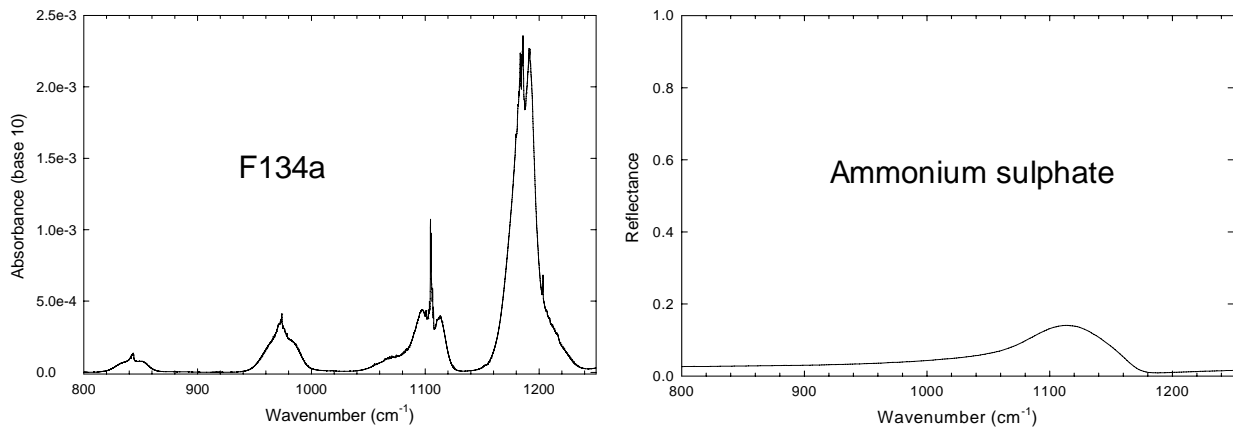


**Figure 8.** Longwave infrared spectral signatures of the gaseous and powdered chemical targets.



**Figure 9.** Weather station mounted at the experimental site near the gas plume generator.

**Table 2.** Meteorological parameters measured during the experiment on April 30, 2009

Time	Air Temp (C)	Wind Dir (0 = N)	Wind speed (km/h)	RH (%)	Radiation	Wind chill
14:50	18.2	194 (from SW)	11	20	844	17
15:10	18.2	132	9.7	16	804	18.1
16:07	18.6	179	11.6	17.3	181	17.2
16:35	18.7	168	11.3	18.1	704	16.7
17:00	18.6	194	12	18.5	473	16

## TEST RESULTS AND DISCUSSION

The Generalized Likelihood Ratio Test (GLRT) was the detection algorithm used to identify the gas plume and other chemical targets in the experiment. This test has been used extensively by DRDC in previous work, and a detailed description of the method is given in references (Manolakis, 2003 & Scharf, 1994). Essentially, the GLRT is described mathematically by:

$$\text{GLRT: } \frac{m^T P_B^\perp m}{m^T P_{BS}^\perp m} = \frac{(P_B^\perp m)^T (P_B^\perp m)}{(P_{BS}^\perp m)^T (P_{BS}^\perp m)} = \frac{\|P_B^\perp m\|^2}{\|P_{BS}^\perp m\|^2}$$

where the numerator represents the squared norm of the measurement,  $m$ , projected out of the background space,  $B$ , and the denominator represents the squared norm of the measurement projected out of the background + signature space,  $S$ . If the measurement does not contain the signature of interest, the result of the GLRT is approximately one.

The detection and identification of F-134a during Pass 2 at a release of 100 L/min on April 30 is shown in Figs. 10A-C. The upper panel in Fig. 10A shows the measured calibrated radiance spectrum (blue curve) and the F-134a reference absorbance spectrum (green curve). The result of projecting the measurement out of the background space is shown by the blue curve in the lower panel of Fig. 10A. This is compared to the projection of the signature out of the background shown by the green curve. The output of the GLRT filter is summarized in Fig. 10B, which shows the detection of F-134a above the threshold level, which was set at ten times the root-mean-square (rms) value of the background result. The detection and identification of the F-134a plume in the image scene is shown in Fig. 10C.

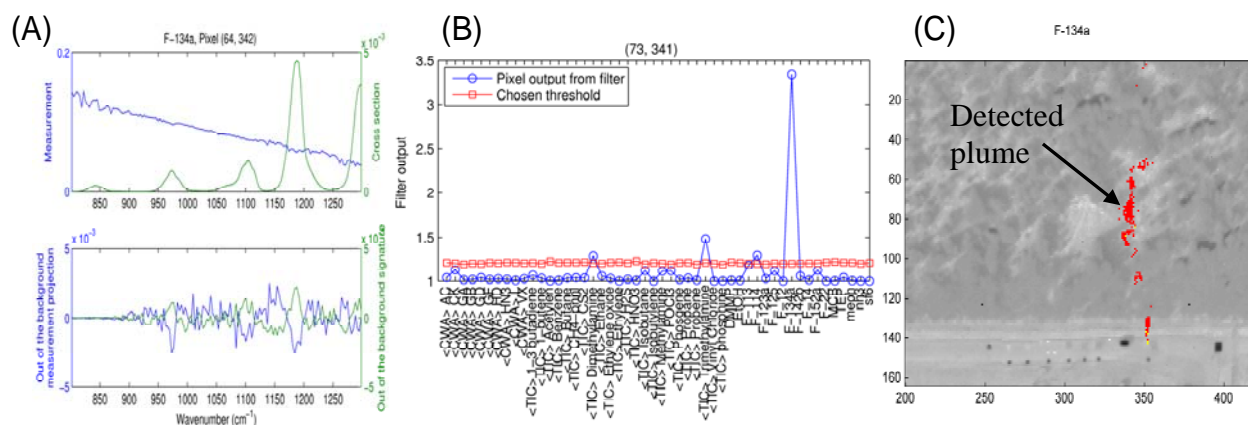


**Figure 10.** The detection and identification of F-134a gas using the GLRT algorithm. The figures are explained in the text.

The detection and identification of ammonium sulphate fertilizer on April 30 is shown in Figs. 11A-C. The upper panel in Figure 11A shows the measured calibrated radiance spectrum (blue curve) and the ammonium sulphate reflectance spectrum (green curve). The result of projecting the measurement out of the background space is shown by the blue curve in the lower panel of Figure 11A. This is compared to the projection of the signature out of the background shown by the green curve. The output of the GLRT filter is summarized in Figure 11B, which shows the detection of ammonium sulphate above the threshold level, which was set at ten times the root-mean-square (rms) value of the background result. The detection and identification of the ammonium sulphate fertilizer in the image scene is shown in Figure 11C.

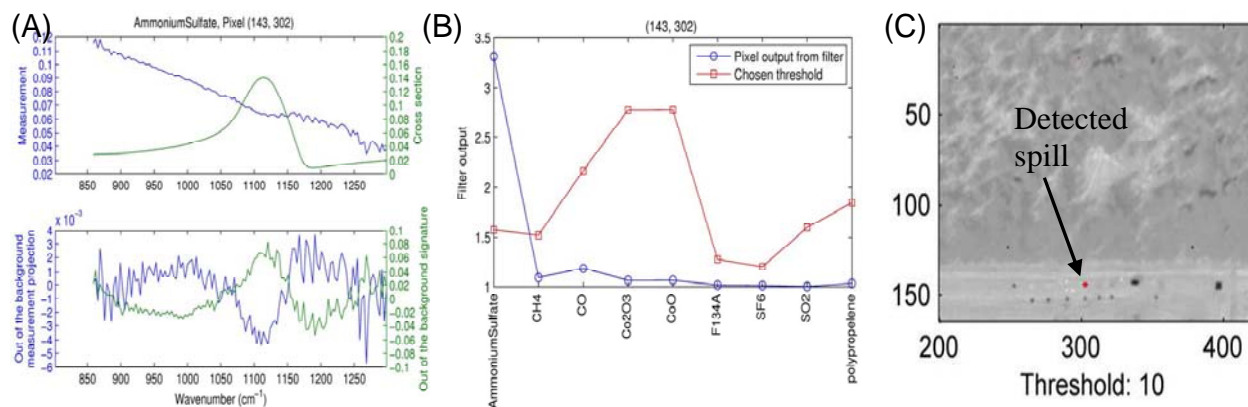


**Figure 11.** The detection and identification of ammonium sulphate fertilizer using the GLRT algorithm. The figures are explained in the text.

## CONCLUSION

Airborne hyperspectral ground mapping is being used in an ever-increasing extent for numerous applications in the military, geology and environmental fields. In particular, mapping in the LWIR region has the potential for detecting identifying chemical vapour plumes and solids.

The Telops Hyper-Cam is a rugged and compact infrared hyperspectral imager based on the Fourier-transform technology. It has been used on the ground in several field campaigns, including the demonstration of standoff chemical agent detection. The Hyper-Cam has been integrated into an airplane to provide airborne measurement capabilities. The system was used most recently in April 2009 during a field measurement campaign at DRDC Valcartier. The results show that the airborne Hyper-cam-LW is able to detect and identify F134a plumes and ammonium sulphate spills. This work builds on previous results obtained under harsh winter conditions in 2008.



## REFERENCES

- Farley, V., Chamberland, M., Lagueux, P., et al., 2007. Chemical agent detection and identification with a hyperspectral imaging infrared sensor, In *Proceedings of SPIE Vol. 6661*, 66610L.
- Puckrin, E., C.S. Turcotte, Lahaie, P., Dubé, D., Farley, V., Lagueux P. and Marcotte F. and Chamberland, M., 2009. Airborne measurements in the infrared using imaging hyperspectral sensors, In *Proceedings of SPIE Vol. 7324-46*, Defense & Security 2009, Orlando, Florida, April 2009.
- Vallières, A., Villemaire, A., Chamberland, M., et al., 2005. Algorithms for chemical detection, identification and quantification for thermal hyperspectral imagers, In *Proceedings of SPIE Vol. 5995*, 59950G.
- Allard, J., Chamberland, M., Farley, V., et al., 2008. Airborne measurements in the longwave infrared using an imaging hyperspectral sensor, In *Proceedings of SPIE Vol. 7086*, 70860K.
- Manolakis, M., Marden, D. and Shaw, G.A., 2003. Hyperspectral image processing for automatic target detection applications, *Lincoln Laboratory Journal*, Vol. 14, 79.
- Scharf, L. and Friedlander, B., 1994. Matched subspace detectors, *IEEE Transactions on Signal Processing*, Vol. 42, 2146.